INVESTIGATING BIOINK HYDROGELS FOR 3D BIOPRINTING TO RECONSTITUTE GLIOBLASTOMA MICROENVIRONMENT

LEONG SHYE WEI

UNIVERSITI SAINS MALAYSIA

2025

INVESTIGATING BIOINK HYDROGELS FOR 3D BIOPRINTING TO RECONSTITUTE GLIOBLASTOMA MICROENVIRONMENT

by

LEONG SHYE WEI

Thesis submitted in fulfilment of the requirements for the degree of Master of Science

FEBRUARY 2025

ACKNOWLEDGEMENT

First and foremost, I would like to express my gratitude to my supervisor, Dr Lee Si Yuen for her guidance, assistance, insight and encouragement throughout my master's programme. Besides, I would like to thank the laboratory technicians and staff from the Central Research Laboratory (School of Medical Sciences), Scanning Electron Microscope Laboratory (School of Health Sciences) and Institute for Research in Molecular Medicine (INFORMM), Universiti Sains Malaysia (USM) for their assistance and providing me with good laboratory environments and facilities during my entire stay. I would also like to express my deepest gratitude to Institute Postgraduate Studies (IPS) for Graduate Student Financial Assistance, Graduated Fellowship and Fundamental Research Grant Scheme (FRGS/1/2020/TK0/USM/02/32–6171275) for the financial support that allowed me to complete my master's study. Last but not least, I would like to express my deepest appreciation to my parents and siblings for their endless love, encouragement, understanding, and belief in me.

TABLE OF CONTENTS

ACK	NOWLED	OGEMENT	ii
TABI	LE OF CO	ONTENTS	iii
LIST	LIST OF TABLESvii		
LIST	OF FIGU	JRES	viii
LIST	OF SYM	BOLS	xii
LIST	OF ABBI	REVIATIONS	xiii
LIST	OF APPI	ENDICES	XV
ABST	RAK		xvi
ABST	RACT		xviii
CHAI	PTER 1	INTRODUCTION	1
1.1	Backgrou	und of the study	1
1.2	Problem	statement/Originality of research	4
1.3	Research	n hypotheses	5
1.4	Research	aim and specific objectives	5
	1.4.1	Specific Objectives	5
1.5	Literatur	e Review	6
	1.5.1	Cellular components of tumour microenvironment	6
	1.5.2	Extracellular matrix (ECM) of glioblastoma	8
	1.5.3	Bioink materials	10
		1.5.3(a) Natural polymers	10
		1.5.3(b) Synthetic polymers	14
	1.5.4	Bioink design and criteria	16
	1.5.5	Bioprinting techniques	19
	1.5.6	Application of 3D bioprinting in glioblastoma	22

CHA	PTER 2	METHODOLOGY	24
2.1	Experim	ental design	24
2.2	Material		25
	2.2.1	Preliminary test	25
	2.2.2	Preparation of alginate (ALG) stock solutions	25
	2.2.3	Preparation of chitosan (CHI) stock solutions	26
	2.2.4	Preparation of alginate-hyaluronic acid (ALG-HA) stock solution	26
	2.2.5	Preparation of chemical crosslinker	26
	2.2.6	Preparation of complete media	27
2.3	3D biop	rinting design	27
2.4	Fabricati	ion of bioink hydrogels at different formulations	30
	2.4.1	Group 1- Formulation of 4% ALG bioinks	30
	2.4.2	Group 2 - Formulation of 4%:0.5% ALG-CHI bioink	31
	2.4.3	Group 3 - Formulation of 4%:0.5%:0.5% ALG-CHI-HA bioinks	32
	2.4.4	Group 4- Formulation of 4% ALG bioinks	33
	2.4.5	Group 5 - Formulation of 4%:0.25% ALG-CHI bioink	34
	2.4.6	Group 6 – Formulation of 4%:0.25%:0.25% ALG-CHI-HA bioinks	
2.5	Evaluati	on of 3D bioprinting parameters	36
2.6	Characte	erisation of physical properties of bioink hydrogels	37
	2.6.1	Porosity Test	37
	2.6.2	Swelling Test	38
2.7	Cell Cul	ture of Glioblastoma	38
2.8	Cell-mat	rix interaction and morphology of bioprinted tumour model	39
	2.8.1	Bioprinting of glioblastoma tumour model	39
	2.8.2	Cell Viability	39

	2.8.3	Scanning Electron Microscopy analysis	40
	2.8.4	Haematoxylin and eosin (H&E) staining	40
2.9	Statistica	al analysis	41
СНА	PTER 3	RESULTS	42
3.1	Formula	tion and fabrication of bioink hydrogels	42
3.2	Evaluation	on of 3D bioprinting parameters	46
	3.2.1	Group 1 – Optimum parameters and POI of 4% ALG	47
	3.2.2	Group 2 – Optimum parameters and POI of 4%:0.25% ALG-CHI	50
	3.2.3	Group 3 – Optimum parameters and POI of 4%:0.25%:0.25% ALG-CHI-HA	53
3.3	Characte	erisation of physical properties of bioink	56
	3.3.1	Porosity Test	56
	3.3.2	Swelling Test	57
	3.3.3	Morphology of 3D bioprinted hydrogels	58
3.4	Cell-mat	rix interaction and morphology of bioprinted cancer models	62
	3.4.1	Cell viability	62
	3.4.2	Microstructure and morphology of 3D bioprinted glioblastoma models	63
		3.4.2(a) SEM	63
		3.4.2(b) H&E	69
СНА	PTER 4	DISCUSSION	73
4.1	Formula	tion and fabrication of bioink hydrogels	73
4.2	Evaluation	on of 3D bioprinting parameters	78
4.3	Characte	erisation of physical properties of bioink	79
4.4	Cell-mat	rix interaction and morphology of bioprinted cancer models	82
СНА	PTER 5	CONCLUSION AND FUTURE RECOMMENDATIONS	87
5.1	Conclusi	on	87

5.2	Recommendations for Future Research	37
REFE	RENCES9)1
APPE	NDICES	
LIST (OF PUBLICATIONS	

LIST OF TABLES

	Page	e
Table 3.1	Printed lines of 4% ALG, 4%:0.5% ALG-CHI, 4%:0.5%:0.5%	
	ALG-CHI-HA pre-crosslink with different concentration of CaCl ₂	
	using the 22G nozzle at 15 kPa pressure	3
Table 3.2	Printed lines of 4% ALG, 4%:0.25% ALG-CHI, 4% ALG-0.25%	
	CHI-0.25% HA pre-crosslink with different concentration of	
	CaCl ₂ using the 22G nozzle at 15 kPa pressure	5

LIST OF FIGURES

	Page
Figure 1.1	Schematic of the complex cellular and non-cellular ECM interactions in the glioblastoma tumour microenvironment. Adapted from Faisal et al., 2022.
Figure 1.2	Chemical structure of alginate. Adapted from Salisu et al., 201611
Figure 1.3	Chemical structure of chitosan. Adapted from El-banna et al., 2019
Figure 1.4	Chemical structure of HA. Adapted from Sionkowska et al., 202013
Figure 1.5	Chemical structure of PEG. Adapted from Ray Foster, 201014
Figure 1.6	Chemical structure of PCL. Adapted from McKeen, 202115
Figure 1.7	Chemical structure of PLA. Adapted from Petinakis et al., 201315
Figure 1.8	Schematic diagram of bioprinting techniques. (A) Extrusion-based Bioprinting (B) Inkjet Bioprinting (C) Laser-assisted Bioprinting and (D) Stereolithography
Figure 2.1	Flow chart of the study24
Figure 2.2	Visualisation of design construct using software, CELLINK HeartWare. (A) number 5 zigzag line for printability and determination of printing speed and printing pressure (B) Top view of the hydrogel construct. (C) Isometric view of a hydrogel construct with size of 5 mm x 5 mm x 1 mm (length x width x height)
Figure 2.3	Schematic of the preparation of 4% ALG using dual syringe mixing
Figure 2.4	Schematic of the of the preparation of 4%:0.5% ALG-CHI using dual syringe mixing. 32
Figure 2.5	Schematic of the of the preparation of 4%:0.5%:0.5% ALG-CHI-

Figure 2.6	Schematic of the of the preparation of 4% ALG using dual syringe mixing
Figure 2.7	Schematic of the of the preparation of 4%:0.25% ALG-CHI using dual syringe mixing
Figure 2.8	Schematic of the of the preparation of 4%:0.25%:0.25% ALG-CHI-HA using dual syringe mixing
Figure 3.1	Printed line of ALG hydrogel with $10 - 17$ kPa printing pressure and $1 - 8$ mm/s printing speed
Figure 3.2	Strand width of 4% ALG. Each data point was the mean of five measurements with triplicate
Figure 3.3	POli of 4% ALG. Data shown means ± standard error of mean of values (n=3). Significant differences were analysed by one-way ANOVA, n.s=non-significant.
Figure 3.4	Printed line of ALG-CHI hydrogel with 10 – 17 kPa printing pressure and 1 – 8 mm/s printing speed.
Figure 3.5	Strand width of ALG-CHI. Each data point was the mean of five measurements with triplicate
Figure 3.6	<i>POli</i> of ALG-CHI. Data shown means \pm standard error of mean of values (n=3). Significant differences were analysed by one-way ANOVA, n.s=non-significant and **p \leq 0.01.
Figure 3.7	Printed line of ALG-CHI-HA hydrogel with 10 – 17 kPa printing pressure and 1 – 8 mm/s printing speed
Figure 3.8	Strand width of ALG-CHI-HA. Each data point was the mean of triplicate five measurements with triplicate
Figure 3.9	<i>POIi</i> of ALG-CHI-HA. Data shown means \pm standard error of mean of values (n=3). Significant differences were analysed by one-way ANOVA, n.s=non-significant and ***p \leq 0.00155
Figure 3.10	Porosity of the ALG, ALG-CHI, and ALG-CHI-HA bioinks. Data shown means \pm standard error of mean of values (n=3). Significant

	differences were analysed by one-way ANOVA, n.s=non-significant, *p \leq 0.05 and ***p \leq 0.00156
Figure 3.11	Swelling ratio of the ALG, ALG-CHI, and ALG-CHI-HA bioinks. Data shown means \pm standard error of mean of values (n=3). Significant differences were analysed by one-way ANOVA, n.s=non-significant, *p \leq 0.05 and **p \leq 0.01
Figure 3.12	3D bioprinted hydrogels of ALG, ALG-CHI and ALG-CHI-HA, incubated in the cell culture conditions, (A) 1 day, (B) 7 days, (C) 14 days, and (D) 21 days without glioblastoma cells
Figure 3.13	SEM of 3D bioprinted (A-B) ALG, (C-D) ALG-CHI, (E-F) ALG-CHI-HA, after immersion in DMEM for 7 days, without glioblastoma cells in surface view (left) and cross-sectional view (right). Scale bar: 200 µm (500x magnification)
Figure 3.14	SEM of 3D bioprinted (A-B) ALG, (C-D) ALG-CHI, (E-F) ALG-CHI-HA, after immersion in DMEM for 21 days, without glioblastoma cells in surface view (left) and cross-sectional view (right). Scale bar: 20 µm (5000x magnification).
Figure 3.15	Absorbance value showing the cell viability of 3D bioprinted ALG, ALG-CHI, and ALG-CHI-HA bioinks. Data shown means \pm standard error of mean of values (n=3). Significant differences were analysed by one-way ANOVA, *p \leq 0.05, **p \leq 0.01, and ***p \leq 0.001.
Figure 3.16	SEM of 3D bioprinted glioblastoma models of (A) ALG, (B) ALG-CHI and (C) ALG-CHI-HA at day 7 of culture with surface view. Formation of cell spheroids (red arrow) and cell protrusions (red box) in bioprinted U87 glioblastoma cells. Scale bar: 200 µm (500x) and 20 µm (5000x).
Figure 3.17	SEM of 3D bioprinted glioblastoma models made of (A) ALG, (B) ALG-CHI and (C) ALG-CHI-HA at day 7 of culture with cross-sectional view. Formation of cell spheroids (red arrow) and cell

	protrusions (red box) in bioprinted U87 glioblastoma cells. Scale
	bar: 200 μm (500x) and 20 μm (5000x)
Figure 3.18	SEM of 3D bioprinted glioblastoma models made of (A) ALG, (B)
	ALG-CHI and (C) ALG-CHI-HA at day 21 of culture with surface
	view. Formation of cell spheroids (red arrow) and cell protrusions
	(red box) in bioprinted U87 glioblastoma cells. Scale bar: 200 μm
	(500x) and 20 µm (5000x)
Figure 3.19	SEM of 3D bioprinted glioblastoma models made of (A)ALG, (B)
	ALG-CHI and (C) ALG-CHI-HA at day 21 of culture with cross-
	sectional view. Formation of cell spheroids (red arrow) and cell
	protrusions (red box) in bioprinted U87 glioblastoma cells. Scale
	bar: 200 μm (500x) and 20 μm (5000x)
Figure 3.20	H&E stained of 3D bioprinted glioblastoma models (4% ALG) in
	(A) day 1 of culture, (B) day 3 of culture, (C) day 7 of culture, (D)
	day 14 of culture, and (E) day 21 of culture. Scale bar: 20 μm ,
	magnification: 40x70
Figure 3.21	H&E stained of 3D bioprinted glioblastoma models (4%:0.25%
	ALG-CHI) in (A) day 1 of culture, (B) day 3 of culture, (C) day 7
	of culture, (D) day 14 of culture, and (E) day 21 of culture. Scale
	bar: 20 µm, magnification: 40x71
Figure 3.22	H&E stained of 3D bioprinted glioblastoma (4%:0.25%:0.25%
	ALG-CHI-HA) in (A) day 1 of culture, (B) day 3 of culture, (C)
	day 7 of culture, (D) day 14 of culture, and (E) day 21 of culture.
	Scale bar: 20 µm, magnification: 40x

LIST OF SYMBOLS

% Percent

°C Degree Celsius

μL Microliter

μm Micrometer

μs Microsecond

cm Centimeter

G Gauge

g Gram

g/cm³ Gram per cubic centimeter

kPa Kilopascal

M Molar

mbar Millibar

mL Milliliter

mm Millimeter

mm/s Millimeter per second

psi Pounds per square inch

v/v Volume per volume

w/v Weight per volume

 ρ Pressure

LIST OF ABBREVIATIONS

2D Two-dimensional

3D Three-dimensional

ALG Alginate

ANOVA Analysis of variance

ATCC American Type Culture Collection

BBB Blood-Brain Barrier

CaCl₂ Calcium chloride

CAD Computer-assisted design

CHI Chitosan

CNS Central nervous system

CO₂ Carbon dioxide

CSCs Cancer stem cells

DMEM Dulbecco's Modified Eagle Medium

DNA Deoxyribonucleic acid

DPX Distyrene, plasticiser and xylene

EBB Extrusion-based bioprinting

ECM Extracellular matrix

EDTA Ethylene diamine tetra acetic acid

EGF Epidermal Growth Factor

EGFR Endothelial Growth Factor Receptor

FBS Fetal Bovine Serum

FDM Fused deposition modelling

FGF Fibroblast Growth Factor

GSCs Glioma stem cells

H&E Haematoxylin and eosin

HA Hyaluronic acid

ILs Interleukins

IPS Institute Postgraduate Studies

iPSCs Induced pluripotent stem cells

LAB Laser-assisted bioprinting

MDSCs Myeloid-derived suppressor cells

MGMT O6-Methylguanine-DNA Methyltransferase

NaCl Sodium chloride

NaOH Sodium hydroxide

NEAA Non-essential Amino Acid

PBS Phosphate Buffer Saline

PCL Poly Caprolactone

PEG Polyethylene glycol

Pen-Strep Penicillin-Streptomycin

PLA Polylactic Acid

POI Parameter Optimisation Index

SEM Scanning Electron Microscope

STL Stereolithography

TGF-β Transforming Growth Factor-beta

TNF-α Tumour Necrosis Factor-alpha

USA United States of America

USM Universiti Sains Malaysia

UV Ultraviolet

WHO World Health Organisation

LIST OF APPENDICES

Appendix A STRAND WIDTH AND POI OF ALG

Appendix B STRAND WIDTH AND POI OF ALG-CHI

Appendix C STRAND WIDTH AND POI OF ALG-CHI-HA

Appendix D POROSITY, SWELLING RATIO AND CELL VIABILITY OF BIOINKS HYDROGEL

PENYELIDIKAN DAKWAT-BIO HIDROGEL UNTUK PERCETAKAN BIO 3D BAGI MEMBENTUK SEMULA PESEKITARAN MIKRO GLIOBLASTOMA

ABSTRAK

Glioblastoma, subjenis glioma yang paling agresif, menghadapi cabaran besar disebabkan ketahanan terhadap ubat, yang mengakibatkan kekerapan berulang dan progresi. Kultur sel dua dimensi (2D) tradisional sering gagal menghasilkan persekitaran mikro tumor yang kompleks dan interaksi selular yang tepat seperti dalam keadaan hidup, yang membatasi keupayaan mereka untuk meramal respons ubat secara tepat. Mengatasi ini, biopencetakan tiga dimensi (3D) muncul sebagai pendekatan moden untuk membina model glioblastoma yang penting untuk ujian pra klinikal ubat. Projek ini bertujuan untuk membina mikropersekitaran glioblastoma menggunakan biopencetakan 3D dan hidrogel. Pelbagai komposisi hidrogel, termasuk alginat (ALG), kombinasi alginat dan kitosan (ALG-CHI), dan campuran alginat, kitosan, dan asid hyaluronik (ALG-CHI-HA), diformulasikan. Sifat fizikal dan interaksi sel-matriks kumpulan bioink ini; ALG, ALG-CHI, dan ALG-CHI-HA — dinilai. Khususnya, hidrogel yang terdiri daripada 4% ALG, 4%:0.25% ALG-CHI, dan 4%:0.25%:0.25% ALG-CHI-HA apabila pra-pengesan dengan 0.102 M CaCl₂ menunjukkan hasil biopencetakan yang paling konsisten dan stabil, menekankan kepentingan menilai komposisi bioink dan parameter penyerapan untuk mencapai hasil pencetakan yang diinginkan. Selain itu, kajian ini menyiasat kesan parameter biopencetakan seperti kelajuan dan tekanan ke atas kualiti konstruk yang dicetak. Keadaan biopencetakan optimum dikenal pasti dengan kelajuan 8 mm/s dan tekanan 10 kPa, memastikan

penyerapan bahan bioink yang tepat dan pemeliharaan integriti struktur. Penilaian porositi menunjukkan trend yang berbeza dari semasa ke semasa: hidrogel ALG mengekalkan porositi stabil (n.s) selepas satu minggu inkubasi DMEM, sementara ALG-CHI (p<0.05) dan ALG-CHI-HA (p<0.001) menunjukkan penurunan yang signifikan dari hari 0 hingga hari 7. Nisbah pembengkakan kekal agak stabil untuk semua kumpulan bioink sepanjang tempoh inkubasi 21 hari, berkisar antara 10.84-14.58. Penilaian sel viabiliti menunjukkan trend yang berbeza: ALG menunjukkan peningkatan awal dari hari 1 hingga 14 diikuti dengan penurunan pada hari 21, sementara ALG-CHI menunjukkan peningkatan viabiliti pada hari 21 (p<0.05), dan ALG-CHI-HA menunjukkan peningkatan viabiliti yang tertunda tetapi signifikan antara hari ke-7 dan ke-21 (p<0.01). Formulasi ALG-CHI dan ALG-CHI-HA mengekalkan viabiliti dari semasa ke semasa, menunjukkan potensi mereka untuk menyokong pertumbuhan dan proliferasi sel jangka panjang. Analisis SEM dan histologi (H&E) memberikan pengesahan visual mengenai morfologi selular dan organisasi dalam konstruk biopencetakan. Kesimpulannya, hidrogel yang dicetak dari semua kumpulan menunjukkan kestabilan dan integriti struktur yang berterusan sepanjang kajian. Di antara formulasi yang berbeza, ALG-CHI menyokong keterhidupan sel glioblastoma yang lebih tinggi dengan pembentukan mikropersekitaran tumor. ALG-CHI-HA juga menunjukkan trend dan prestasi yang serupa. Oleh itu, ALG-CHI dan ALG-CHI-HA sesuai digunakan untuk kultur sel 3D jangka panjang.

INVESTIGATING BIOINK HYDROGELS FOR 3D BIOPRINTING TO RECONSTITUTE GLIOBLASTOMA MICROENVIRONMENT

ABSTRACT

Glioblastoma, the most aggressive glioma subtype, presents significant challenges due to drug resistance, resulting in frequent recurrence and progression. Traditional two-dimensional (2D) cell cultures often fail to replicate accurately the complex tumor microenvironment and cellular interactions found in vivo, thereby limiting their ability to predict drug response reliably. Addressing this issue, threedimensional (3D) bioprinting emerges as a modern approach for constructing glioblastoma models, vital for preclinical drug testing. This project aims to fabricate a glioblastoma microenvironment using 3D bioprinting and hydrogels. Various hydrogel compositions; alginate (ALG), a combination of alginate and chitosan (ALG-CHI), and a blend of alginate, chitosan, and hyaluronic acid (ALG-CHI-HA) — were formulated. The physical properties and cell-matrix interactions of these bioink groups (ALG, ALG-CHI, and ALG-CHI-HA) were assessed. Notably, hydrogels composed of 4% ALG, 4%:0.25% ALG-CHI, and 4%:0.25%:0.25% ALG-CHI-HA, when precrosslinked with CaCl2 at the concentration of 0.102 M, they exhibited the most consistent and stable bioprinting results, highlighting the importance of evaluating different bioink compositions and crosslinking parameters to achieve the desired printing outcomes. Furthermore, the study investigated the impact of bioprinting parameters, such as speed and pressure on the quality of the printed constructs. Optimal bioprinting conditions were identified with a printing speed of 8 mm/s and printing pressure of 10 kPa, ensuring precise deposition of bioink materials and maintenance of structural integrity. Porosity assessments demonstrated varying trends

over time. ALG hydrogels maintained stable porosity (n.s) after one week of DMEM incubation, whereas ALG-CHI (p<0.05) and ALG-CHI-HA (p<0.001) showed significant decreases in porosity from day 0 to day 7. Swelling ratios remained relatively stable for all bioink groups throughout the 21-day incubation period, ranging between 10.84-14.58. Cell viability assessments revealed distinct trends: ALG demonstrated an initial increase from day 1 to 14, followed by a decrease at day 21 (p<0.001). Conversely, ALG-CHI showed increased in cell viability at day 21 (p<0.05), and ALG-CHI-HA exhibited delayed but significant increased viability between days 7 and 21 (p<0.01). ALG-CHI and ALG-CHI-HA formulations sustained viability over time, suggesting potential for supporting long-term cell growth and proliferation. SEM and histological (H&E) analyses provided valuable visual confirmation into the cellular morphology and organisation within the bioprinted constructs. In conclusion, the bioprinted hydrogels from all groups demonstrated persistent stability and structural integrity throughout. Among the different formulations, ALG-CHI supported higher viability of glioblastoma cells with formation of tumour microenvironment. ALG-CHI-HA also showed similar trend and performance. Hence, ALG-CHI and ALG-CHI-HA are suitable to be used for longterm 3D cell cultures.

CHAPTER 1

INTRODUCTION

1.1 Background of the study

Glioblastoma (World Health Organisation (WHO) grade IV glioma), stands as the most common primary brain cancer. This type of cancer is exceptionally aggressive, and representing the most malignant category among gliomas (Gómez-Oliva et al., 2021; Stanković et al., 2021). Patients diagnosed with glioblastoma face a poor prognosis with a median survival time of approximately 15 months for newly diagnosed cases and 5–7 months for recurrent cases. Moreover, the five-year survival rate can be as low as 6.8% (Dai et al., 2016; Ostrom et al., 2021). Due to its microscopic nature, characterised by abnormal cellular, microbial, or molecular changes at a cellular or molecular level, glioblastoma may not manifest noticeable symptoms or visible changes in affected individuals, complicating diagnosis without specialised laboratory tests. Glioblastoma is considered as microscopic disease because symptoms may not arise or be detectable on imaging studies until the disease has progressed significantly. Therefore, complete tumour excision is often impractical due to the cancer's highly invasive characteristics, leading to persistent disease despite surgery. Patients typically receive radiation and chemotherapy following surgery (O. G. Taylor et al., 2019). Nevertheless, further research in drug discovery and development is crucial to improve the existing glioblastoma therapeutics.

In drug screening, two-dimensional (2D) cell cultures and animal models are commonly used to assess drug safety and efficacy before clinical trials. However, monolayer cancer cell cultures represent a simplified *in vitro* model that does not fully address many physiological questions due to the complexity of the tumour microenvironment. Besides biochemical signalling, various physical factors such as

stiffness of extracellular matrix (ECM), interstitial flow, shear stresses, and fluid dynamics can impact the tumour development (Tiwari et al., 2021). Therefore, improved 3D tumour models are needed to study glioblastoma and its responses to drugs.

Conventional methods for constructing 3D *in vitro* models have traditionally relied on scaffold-based techniques and microfabrication approaches. Scaffold-based methods involve seeding cells onto preformed scaffolds that provide structural support and cues for tissue formation. However, these scaffolds often lack precise control over the microarchitecture, which can lead to inhomogeneous cell distribution and limited mimicry of native tissue environments. Microfabrication approaches utilise microengineering technologies to create complex tissue structures with high spatial resolution. For example, photolithography uses light to pattern a photosensitive material, allowing for the creation of precise 2D and 3D structures. Microfluidics involves the manipulation of small volumes of fluids within microscale channels, enabling the precise control over the spatial organisation of cells and biomaterials, which is essential for creating heterogeneous tissue constructs. Despite their advantages, these methods are often labour-intensive, expensive, and require specialised equipment.

Over the past few decades, 3D bioprinting has emerged as a promising technology in cancer research, enabling the creation of advanced cellular models. This innovative approach utilises computer-assisted design (CAD) software to deposit biobased material(s) or bioinks layer by layer, aiming to replicate the natural ECM of human organs using biocompatible materials that are embedded with living cells, growth factors, or hormones (Zadpoor and Malda, 2017). Remarkably, 3D bioprinting

shows potential in addressing various medical research challenges and has found applications in disease modelling, regenerative medicine, and the development of functional organ replacement.

In a nutshell, the rapid development of 3D bioprinting offers an advance option for the glioblastoma cancer research. In this research study, we aim to formulate a novel bioink with the combination of alginate, chitosan and hyaluronic acid to construct glioblastoma microenvironment using 3D bioprinting.

While each of these materials offers unique advantages, they also have individual limitations. Alginate, for example, is widely used for its ease of gelation and biocompatibility but lacks cell-adhesive properties and has limited mechanical strength (K. Y. Lee and Mooney, 2001). Chitosan, on the other hand, provides excellent biocompatibility and biodegradability, but its acidic nature can hinder cell viability, and its low mechanical properties limit its use in applications requiring structural support (Croisier and Jérôme, 2013). Hyaluronic acid is an excellent material for mimicking ECM components and promoting cell migration, but it lacks the structural stability required for supporting complex tissue architectures (Burdick and Prestwich, 2011). By combining these three bioinks, we aim to leverage the strengths of each material while mitigating their individual drawbacks: alginate provides the gelation and structural framework, chitosan offers enhanced biocompatibility and biodegradability, and hyaluronic acid enhances cell-ECM interactions and tissue formation. This novel bioink combination remains relatively unexplored, and its optimisation and evaluation for physical properties and cell response will contribute to creating a more functional and physiologically relevant glioblastoma model.

1.2 Problem statement/Originality of research

The low success rate of 3.4% in oncology clinical trials, reported by Wong et al., (2019), highlights the significant challenges in drug development. One factor that may contribute to these challenges is the reliance on 2D monolayer cultures of cancer cells in the early stages of preclinical studies. These 2D culture systems, while valuable for initial drug screening and testing, may not fully replicate the complexity of human tumours, which could impact the subsequent stages of drug development and clinical trials. This limitation highlights the necessity for more physiologically relevant models, such as 3D cell cultures or animal models, which better mimic the intricacies of tumour biology and can potentially enhance the translational success of drug development efforts.

3D bioprinting technology is rapidly advancing in cancer disease modelling to replicate the architecture and microenvironment of tumour tissues. Furthermore, 3D cell culture models derived from human cells offer a more direct representation of human biology compared to animal models. This human relevance can lead to better predictions of human responses to drugs and therapies. However, studies using 3D bioprinting technology for glioblastoma are limited, primarily utilising uniform bioink materials, notably alginate alone (Chaicharoenaudomrung et al., 2019; Haring et al., 2020; Utama et al., 2020; X. Wang et al., 2018b) or in combination with gelatine and fibrin (Dai et al., 2016; Han et al., 2020; X. Wang et al., 2018a, 2019). Challenges remain in identifying appropriate bioink, controlling bioprinted tissue dimension, and improving post-bioprinting cell survival rate, among others. These obstacles must be addressed before a truly cancer-mimicking model can be integrated into pharmaceutical industrial settings. A critical factor for simulating the native tumour microenvironment in cancer disease modelling is the use of a well-designed biomimetic bioink.

1.3 Research hypotheses

- 1. The ideal bioink consists of optimum formulation and components to form a desired 3D *in vitro* model with appropriate printing parameters.
- 2. The bioink exhibits sufficient porosity to support the viability of glioblastoma cells in long-term culture.
- 3. The bioprinted glioblastoma 3D microenvironment demonstrate increased cell viability and characteristic features as the culture period progresses.

1.4 Research aim and specific objectives

The aim of this study is to construct glioblastoma microenvironment using 3D bioprinting and hydrogels for future cancer drug screening. This project contributes to achieving the 'Sustainable Development Goals' (SDG 3 – Good Health and Well-being) set by the Ministry of Higher Education, focusing on the 10-10 MYSTIE Framework by exploring the application of technology drivers 'Advances Materials and Bioprinting' for the socio-economic drivers in Malaysia, including 'Medical and Healthcare' and 'Smart Technology and Systems'.

1.4.1 Specific Objectives

- To determine the optimum bioink formulation and bioprinting parameters (speed and pressure) for the fabrication of a novel bioink.
- 2. To evaluate the physical properties of the bioink, including the swelling ratio and porosity.
- 3. To investigate the cell viability and cell-matrix interaction of the bioprinted scaffold on glioblastoma cell behaviour.

1.5 Literature Review

1.5.1 Cellular components of tumour microenvironment

The cellular components of glioblastoma consist of malignant cells, including tumour cells and various invasive peripheral immune cells, as well as healthy brain cells such as neurons, neuroglia, pericytes, and endothelial cells. The non-malignant cellular part comprises local immune cells such as microglia and astrocytes, as well as lymphocytes and endothelial cells (Faisal et al., 2022).

Glioma cells are believed to originate from altered glial progenitors and exhibit various subtypes based on their level of differentiation, such as astrocytomas, oligodendrogliomas, and ependymomas (Canoll and Goldman, 2008; Riemenschneider et al., 2010). These cells can form tumour throughout the brain and spread diffusely into nearby parenchymal tissue, infiltrating along existing brain structures (Claes et al., 2007). They invade brain tissue through ECM components such as myelinated fibers and brain vasculature (Giese et al., 2003). Additionally, glioma cells can migrate into the subarachnoid region through perivascular space (Engelhardt et al., 2017). Due to their extensive invasion, surgical resection alone often proves insufficient for a cure, as cells persist and regenerate from invasion sites beyond the resection boundaries (L. P. Taylor, 2010).

Glioma stem cells (GSCs) possess high tumorigenicity, invasiveness, and resistance to various treatments (Holland, 2001). They are often found in the "vascular niche" surrounding tumour blood vessels, where they receive microenvironmental cues supporting their stem-like properties, enhance invasion, and promote resistance to treatment (Cheng et al., 2013). The cancer stem cells (CSCs) theory, increasingly validated over the past two decades in glioblastoma and other cancers, proposes that self-renewing CSCs initiate and sustain tumour development (Sengupta et al., 2023;

Shimokawa et al., 2017; Singh et al., 2004). GSCs exhibit long-term proliferation, self-renewal, differentiation, and a dormant state (G0 phase), forming tumour spheres in culture due to their ability to generate clones and recapitulating the original tumour phenotype when transplanted into mice. Because of their self-renewing capacity and persistent replication, GSCs are recognised as the primary "units of selection" driving tumour growth (Greaves, 2013).

Astrocytes are the predominant brain cells and play a pivotal role in glioblastoma (O'Brien et al., 2013). Tumour-associated astrocytes stimulate the release of degradative enzymes, cytokines, chemokines, and growth factors, which in turn enhance glioblastoma proliferation, survival, and invasion of brain parenchyma. The Janus kinase (JAK)/signal transducer and activator of transcription (STAT) pathway is a key signalling pathway that regulates immune responses, cell growth, and survival. Inhibition of the JAK/STAT signalling pathway skews the balance of pro- and antiinflammatory cytokines towards a pro-inflammatory state. The intricate interaction between astrocytes and microglial cells suggests that tumour-associated astrocytes may anti-inflammatory responses, thereby contributing foster further the immunosuppressive microenvironment characteristic of gliomas (Ellert-Miklaszewska et al., 2013; Henrik Heiland et al., 2019).

In the normal brain, macrophages are a minority but play a crucial role in coordinating the immune response during abnormal conditions. They are recruited to the brain as the tumour form (Bowman et al., 2016) or differentiate into macrophages after being recruited as monocytes into the tumour microenvironment (Z. Chen et al., 2017). Glioblastoma-induced disruption of the Blood-Brain Barrier (BBB) allows their entry into the brain (Desland and Hormigo, 2020). Microglia, as resident immune cells of the central nervous system (CNS), exhibit pro-angiogenic behaviour (Brandenburg

et al., 2016). The reactions of microglia to various neuropathologies have also been associated with BBB disruption (da Fonseca et al., 2014). Neutrophils might contribute to resistance against anti-angiogenic therapy, potentially clarifying the correlation between neutrophil infiltration and glioma grade (Liang et al., 2014). This correlation could also arise from their activation of tumour growth and invasion via neutrophil extracellular traps (Zha et al., 2020).

Myeloid cells constitute the predominant immune cell population within the glioma microenvironment, comprising approximately 60% of all infiltrating immune cells (Chang et al., 2016; Simonds et al., 2021). This population includes resident microglia, bone marrow-derived macrophages, myeloid-derived suppressor cells (MDSCs), dendritic cells, and neutrophils (Chen and Hambardzumyan, 2018). Although microglia and macrophages share certain phenotypic characteristics, they can be distinguished by specific cellular markers despite their distinct developmental origins. Microglia, constituting around 10% of the brain cell population, originates from yolk sac erythro-myeloid progenitors during early embryonic development and is essential for maintaining brain homeostasis (Alliot et al., 1999). However, under pathological conditions, they tend to polarise into two main categories: neurotoxic and neuroprotective, exhibiting changes in both morphology and marker expression (Jang et al., 2013).

1.5.2 Extracellular matrix (ECM) of glioblastoma

The ECM, part of the non-cellular components in the tumour microenvironment, not only provides structural support to cellular component but also initiates biochemical and biomechanical signals which is crucial for tissue morphogenesis, differentiation, and homeostasis. The ECM is composed of minerals, interstitial fluid, fibrous proteins (such as collagen and elastin, which provide tensile strength), and glycoproteins

(fibronectin, laminin, and tenascin). Proteoglycans such as heparan sulfate, chondroitin sulfate, and keratan sulfate, as well as glycosaminoglycans such as hyaluronic acid, are the components of the non-fibrillar ECM (Frantz et al., 2010). Figure 1.1 illustrates the schematic diagram of complex interactions between cellular and non-cellular components of the ECM within the glioblastoma tumour microenvironment.

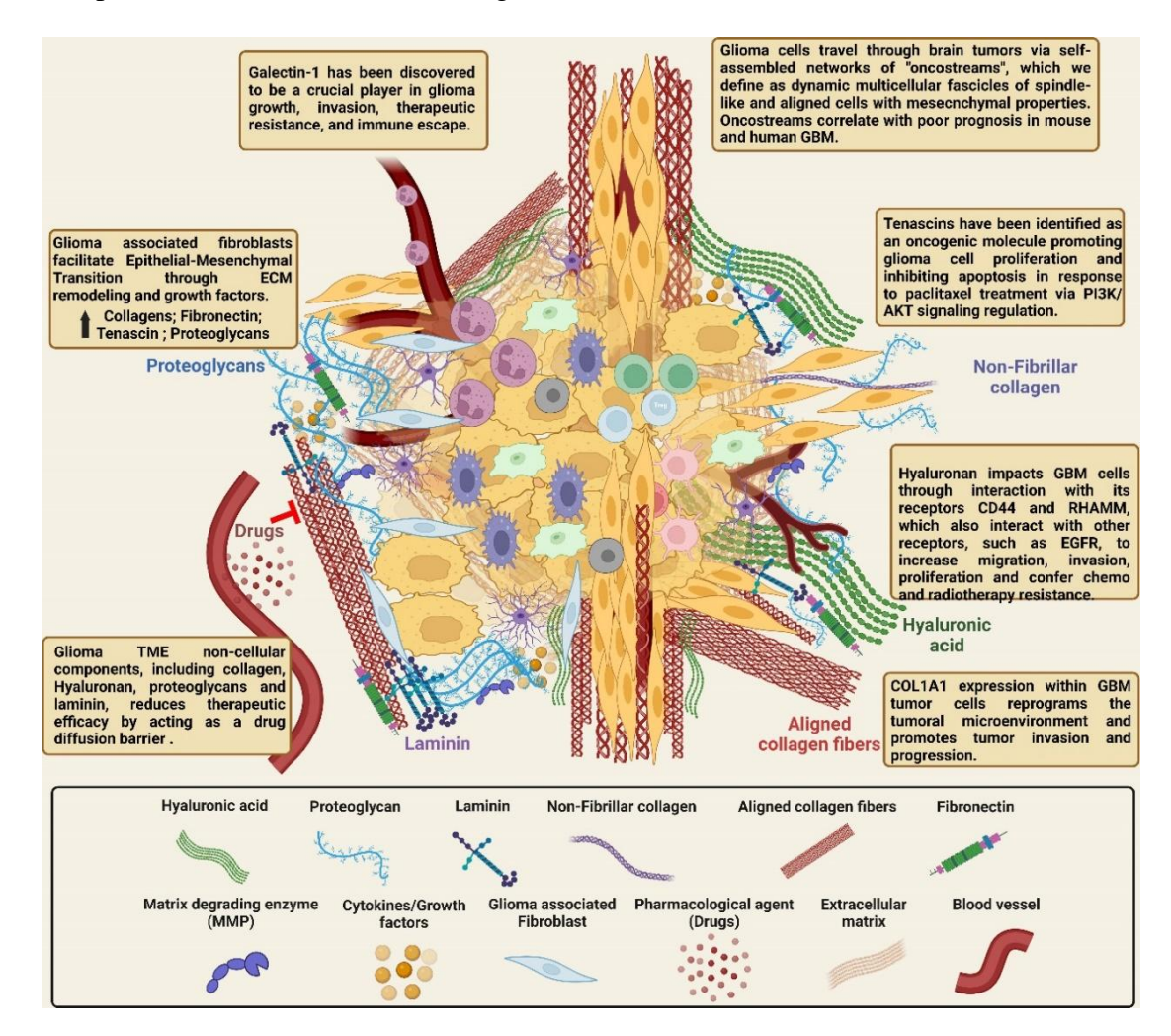


Figure 1.1 Schematic of the complex cellular and non-cellular ECM interactions in the glioblastoma tumour microenvironment. Adapted from Faisal et al., 2022.

The ECM of the brain differs from that of other organs because it contains comparatively fewer fibrotic ECM proteins, such as collagen, fibronectin, and laminin. These proteins are mainly located at the meninges and in the basal membrane surrounding blood vessels. However, glycosaminoglycans (like hyaluronic acid), proteoglycans, and other connecting proteins are abundant in brain parenchyma (Novak

and Kaye, 2000; Rauch, 2007). The ECM is altered in glioblastoma tumour compared to healthy brain tissue, and it is essential for tumour invasion and migration. Increased levels of collagen, hyaluronic acid, fibronectin, laminin, tenascin C, and vitronectin have been demonstrated to play significant roles in the development and progression of glioblastoma (Bellail et al., 2004; Tamai et al., 2022).

1.5.3 Bioink materials

Hydrogels are essential in 3D bioprinting as they replicate the physical and biochemical environment of native ECM. Hydrogels are made up of hydrophilic polymer chains which can be structured into various shapes and sizes, capable of absorbing water up to a thousand times their dry weight. Hydrogels used in bioprinting must meet specific physical and biological requirements in the cellular microenvironment. They must be biocompatible, meaning the material can function appropriately with a host response in a specific situation. This includes being weakly immunogenic, meaning the hydrogel should not trigger a strong immune response that could lead to inflammation or rejection by the body. Additionally, the material's degradation by-products must be non-toxic, ensuring that any breakdown products of the hydrogel are harmless and do not cause damage to surrounding tissues or cells (Seliktar, 2012; Williams, 2008).

1.5.3(a) Natural polymers

Alginate is an anionic linear homopolymer composed of (1,4)-linked β -d-mannuronate (M units) and α -l-glucuronic acid (G units), which can be found in the cell walls of brown algae. Figure 1.2 shows the chemical structure of alginate. It exhibits significant water absorption due to its high carboxylic acid content. Introducing divalent cations (e.g., calcium, barium, strontium) facilitates rapid cross-linking between the G blocks of adjacent polymer strands (Vanderhooft et al., 2007). Mammals do not produce

alginase, thus preventing enzymatic degradation of alginate hydrogels. However, they can be degraded when divalent cations are replaced by monovalent cations (e.g., sodium) in the surrounding environment. This degradation mechanism is crucial for biocompatibility because alginate polymer strands are too large to be filtered by the kidneys for clearance, and excessive displacements of calcium can potentially cause transient local hypercalcemia. Animal studies using alginate hydrogels have shown no adverse events, and these hydrogels have demonstrated low to no immunogenicity (Orive et al., 2002). Furthermore, alginate hydrogels can be modified to degrade in aqueous media when partially oxidised, if necessary (Merceron and Murphy, 2015a). Sabetta et al., (2023) examined the response of DU145 (prostate cancer cells) and U87 (glioblastoma cells) to dasatinib treatment, cultured in a model of 3D spheroids and 3D bioprinted structures using alginate/gelatine. Both DU145 and U87 cells proliferated and formed cell spheroid aggregates in 3D alginate/gelatine bioprinted structures over two weeks. Dasatinib treatment revealed that cells bioprinted in 3D were significantly more resistant to drug toxicity compared to cells cultured in 2D monolayers, which was comparable with the behaviour observed in the 3D spheroids model (Sabetta et al., 2023).

Figure 1.2 Chemical structure of alginate. Adapted from Salisu et al., 2016.

Chitosan, a natural cationic copolymer of β -(1-4) linked 2-acetamino-2-deoxyd-glucopyranose and 2-amino-2-deoxy-d-glucopyranose, is the deacetylated form of chitin derived from crustacean shells. Figure 1.3 demonstrates the chemical structure of chitosan. Research on cell-laden 3D printed structure using chitosan-based hydrogels has been limited due to the acidic nature of the gel. Chitosan only dissolves in weak acids such as acetic acid, and the pH (around 4.0) of the solution is not favourable for living cells. Several studies have explored encapsulating cells within chitosan-based scaffolds by incorporating them with other natural and synthetic hydrogel systems and adjusting the pH to neutral levels (Unagolla and Jayasuriya, 2020). However, the electrostatic interaction of protonated NH₃⁺ in chitosan allows penetration of electrons into negatively charged bacterial membrane, resulting in bacterial death or growth restriction, demonstrating good antibacterial characteristics (Logithkumar et al., 2016). Chitosan-derived bioinks exhibit sufficient mechanical strength to support the viability of enclosed cells, creating a microenvironment similar to natural tissue, and gradually yielding to the ECM produced by the cells (D. Lee et al., 2018). Erickson et al. reported that all chitosan-hyaluronic acid scaffolds supported glioblastoma proliferation over a 12-day culture period; however, scaffolds with increasing stiffness produce larger spheroids. Moreover, glioblastoma cells grown on stiffer chitosan-hyaluronic acid scaffolds showed significantly higher resistance to the chemotherapy drug temozolomide (Erickson et al., 2018).

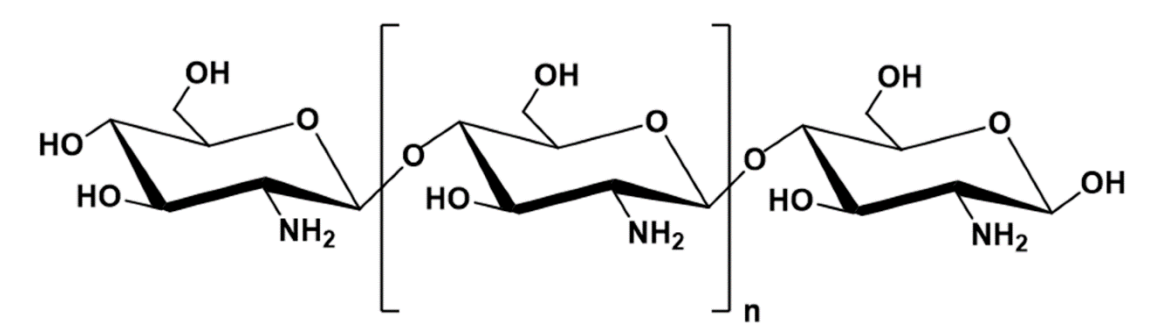


Figure 1.3 Chemical structure of chitosan. Adapted from El-banna et al., 2019.

Hyaluronic acid (HA) is composed of repeating units of the disaccharide: β -1,4β-1,3-N-acetyl-D-glucosamine, D-glucuronic acidan anionic, nonsulfated glycosaminoglycan. Figure 1.4 shows the chemical structure of HA. HA is found in the ECM, vitreous humour, and synovial fluid of articulating joints in the body. Due to its roles in cell signalling, wound repair, cell morphogenesis regulation, and matrix organisation, HA-based biomaterials are attractive for clinical products (Prestwich, 2011). Furthermore, HA has significant immunomodulatory and anti-inflammatory effects, prompting research into its use as an anti-adhesion agent in abdominal and connective tissue procedures (Merceron and Murphy, 2015a). High levels of HA have been correlated with poor prognosis of glioblastoma patients (Tammi et al., 2008). Molecularly, HA binds to membrane receptors essential for glioma cell invasion, motility, and inflammation, such as the receptor for hyaluronan-mediated motility (RHAMM) and the glycoprotein receptor CD44 (Alghamri et al., 2021; Pibuel et al., 2021). Tavakoli et al., (2023) modified HA with cysteine and aldehyde functional groups to create hydrogels with dual cross-linking of disulfide and thiazolidine products. They reported that the bioink maintained in shape and enhanced biological properties, supporting high cell survival post-printing with more than two-fold increase in stemness marker (OCT3/4 and NANOG) of human mesenchymal stem cells, promoting cell proliferation and migration (Tavakoli et al., 2023).

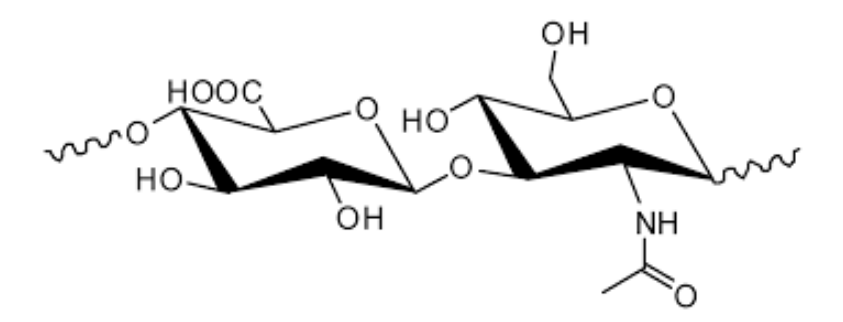


Figure 1.4 Chemical structure of HA. Adapted from Sionkowska et al., 2020.

1.5.3(b) Synthetic polymers

Polyethylene glycol (PEG) is a hydrophilic polymer synthesised through radical polymerisation reactions. It exhibits a linear or branched structure with asymmetric or dissymmetric hydroxyl end groups, as shown in Figure 1.5. Due to its enhanced biocompatibility, PEG finds wide application in drug delivery systems, tissue engineering scaffolds, and surface modification to create amphiphilic block copolymers and ionomers (Ulbricht et al., 2014; Zhu, 2010). PEG naturally resists protein adsorption and cell adhesion, primarily forming hydrogels. However, its nonbiodegradability and low mechanical strength are notable drawbacks, attributed to its C-C polymer backbone. Nonetheless, PEG degradation typically occurs through hydrolytic and enzymatic processes (Alcantar et al., 2000; Romberg et al., 2005; Zhu, 2010).

Figure 1.5 Chemical structure of PEG. Adapted from Ray Foster, 2010.

Poly Caprolactone (PCL) possesses advantageous bioink qualities, such as stiffness, biocompatibility, and degradability, at a relatively lower cost (Murphy and Atala, 2014; Woodruff and Hutmacher, 2010). Figure 1.6 illustrates the chemical structure of PCL. It stands out as a non-toxic polymers, maintaining considerable stability for up to 6 months and having a biological half-life of approximately 3 years (Pan et al., 2020). Selective laser sintering printed PCL scaffolds exhibit features such as a porous structure promoting interconnectedness, a rough surface texture, and a density similar to bone, which facilitates bone regeneration and cell ingrowth. However,

its prolonged biological half-life poses challenges for scaffolds in applications other than bone tissue engineering. Additionally, its high hydrophobicity leads to reduced bioactivity, resulting in slower cell proliferation and tissue adhesion (Gonçalves et al., 2016; Guvendiren et al., 2016).

Figure 1.6 Chemical structure of PCL. Adapted from McKeen, 2021

Polylactic Acid (PLA) is an aliphatic polyester that degrades through hydrolysis, possessing notable attributes such as biocompatibility, degradability, and printability, rendering it a prominent choice for polymeric bioink (Serra et al., 2013). Figure 1.7 shows the chemical structure of PLA. In fused deposition modelling (FDM) technique, PLA serves as the primary polymer precursor, producing filaments suitable for musculoskeletal tissue engineering applications, including ligament substitution and nonbiodegradable fibre replacement. However, PLA's degradation releases acidic byproducts, compromising its long-term biocompatibility by triggering tissue inflammation and cell death (Asti and Gioglio, 2014; Guvendiren et al., 2016).

Figure 1.7 Chemical structure of PLA. Adapted from Petinakis et al., 2013.

1.5.4 Bioink design and criteria

A bioink functions similarly to ink used in traditional printers, but instead of conventional dyes, it utilises biological substances to produce 3D structures. The primary component of bioink is hydrogels, which are water-rich polymers capable of forming a gel-like consistency. These hydrogels closely mimic the natural ECM. The selection of materials for bioinks is critical to ensure successful 3D printing and the subsequent formation of functional tissues (Skeldon et al., 2018). One of the key considerations in bioink design is selecting suitable biomaterials that provide structural integrity and appropriate mechanical properties to support cell growth and tissue formation (Murphy and Atala, 2014).

In the bioprinting process, crosslinking is a crucial step which involves transitioning a biomaterial solution or bioink into a gelled or crosslinked hydrogel. Crosslinking process occurs where polymer chains are linked together using physical methods (including ionic interactions and hydrogen bonding) or chemical reactions (which forms covalent bonds through photoinitiation or enzyme-catalysed reactions), resulting in the formation of a stable polymeric network within the hydrogel (Merceron and Murphy, 2015b). Various crosslinking methods are utilised, including ionic crosslinking (a physical process, such as calcium ions for alginate), thermal crosslinking (a physical process, using heat to induce gelation), photo-crosslinking (a chemical process, using UV light to initiate polymerization), and enzyme crosslinking (a chemical process, using enzymes to catalyse polymerisation).

Ionic crosslinking occurs when a charged polymer, soluble in water, binds with ions of the opposite charge. Alginate is a prominent example that can be crosslinked by divalent metal ions like Ca²⁺, Ba²⁺, and Zn²⁺ (Sarker et al., 2018). Commonly, water-soluble calcium salts such as calcium chloride, calcium sulphate, and calcium carbonate

are employed for crosslinking in ionic crosslinking. The addition of Ca²⁺ ions or other di/trivalent cations induces rapid gelation of the solution. However, this method has drawbacks such as limited mechanical strength and the potential release of metal ions into the body post-implantation (Freeman and Kelly, 2017; Naghieh et al., 2020).

Thermal crosslinking, on the other hand, occurs in polymers sensitive to temperature. Altering temperature levels can initiate crosslinking or gelation. Polymers like agarose, gelatine, and collagen undergo thermal crosslinking, with a gel transition temperature below which the solution solidifies. However, gels formed through this method are typically mechanically weak (Chen et al., 2023).

Photo crosslinking involves the photo-induced formation of a covalent bond between macromolecules, yielding a crosslinked network. Photo-curable polymers can form 3D hydrogels when exposed to laser or visible light. Proteinaceous biopolymers containing tyrosine residues, such as collagen, fibrin and gelatine, require an appropriate photoinitiator for photo-crosslinking (Sando et al., 2011). While many polymers cannot be directly crosslinked by light, they can be made photo-crosslinkable by reacting with acrylate- or methacrylate-based agents. These polymers are typically crosslinked using UV light at wavelengths of 320-365 nm. However, UV light poses potential biological risks and may harm both cells within the printed constructs and operators (Izadifar et al., 2018).

Enzyme crosslinking involves utilising enzymes as catalysts to create covalent bonds between protein-based polymers. This approach is promising for bioprinting due to the gentle nature of enzymatic reactions, which helps maintain cell viability. Various enzymes, including microbial transglutaminase, tyrosinase, and horseradish peroxidase, have been employed in bioprinting to form hydrogels from materials such as HA, gelatine, fibrinogen, polypeptides, and chitosan (Gantumur et al., 2020). However, the

challenges of this crosslinking method include acquiring the necessary enzymes, limited mechanical properties of resulting hydrogels, and sensitivity to environmental conditions such as temperature and pH (Naranjo-Alcazar et al., 2023; Züger et al., 2023).

The stability of the bioprinted structures play a pivotal role in the bioprinting procedure. When using bioinks with low viscosity, the precision of the printed structure may diminish due to ink spreading. Additionally, inadequate crosslinking parameters can affect structure resolution: insufficient crosslinking can cause spreading of the structure, while excessive crosslinking may result in layering and the failure to integrate the entire structure properly. The bioink should possess sufficient mechanical strength for the initial printed layers to support subsequent deposition, preventing collapse or any compromise to the structure (Tabriz et al., 2015, 2017).

Swelling and contractile behaviours of materials are critical factors in tissue engineering fabrication. Materials that swell excessively may absorb fluid from surrounding tissues, while contraction could lead to the closure of essential pores or vessels necessary for cell migration and nutrient delivery. Understanding these material responses is crucial, especially when employing multiple materials with varying swelling or contractile properties, as it could compromise layer integrity or deform of the final construct (Murphy and Atala, 2014).

Understanding and optimising cell density is important in bioink design. Cell density affects cell behaviour and formation of ECM, thereby influencing the functionality of bioprinted constructs. A structure with a very low cell density may fail to sustain the tumour growth due to insufficient cell-cell interactions, whereas excessively high cell density can lead to cell overcrowding, potentially resulting in tissue necrosis or cell death (Cidonio et al., 2019; Karvinen and Kellomäki, 2023).

However, defining what constitutes high or low cell density lacks consensus, as it varies depending on factors such as the specific bioprinting technique, cell type utilised, and desired characteristics of the final product. Ultimately, the core of bioink design lies in formulating biomaterial-based inks capable of supporting cell viability, proliferation, and differentiation throughout the printing process and post-printing cultivation (Murphy and Atala, 2014).

1.5.5 Bioprinting techniques

In recent decades, 3D printing, an additive manufacturing-based technique has emerged as cutting-edge technology widely adopted across industries including manufacturing, engineering, and biomedical field. In 1986, Charles Hull patented stereolithography (STL), a method for printing ultraviolet (UV)-curable materials layer by layer (Hull, 1986), laying the groundwork for various other 3D printing systems such as, inkjet bioprinting, extrusion-based bioprinting (EBB), laser-assisted bioprinting (LAB), and vat polymerisation.

A bioprinter is an important component of bioprinting. The 3D bioprinting process relies on four main printing technologies: inkjet-based, extrusion-based, light-assisted bioprinting, and STL (Figure 1.8). Because specific bioinks influence the integration of living cells in the final bioprinted product, the choice of printing technology impacts not only the selection of suitable bioink but also the complexity of architectural features achievable in the final bioprinted object.

In recent years, extrusion-based bioprinting, also known as direct writing, has become widely attractive in biofabrication and tissue engineering. Extrusion bioprinting utilises pneumatical force (gas or pressurised air) and mechanical force (screw or piston) to extrude the material (Figure 1.8A). This method is suitable for high cell density material or high viscosity material. Pneumatically driven printers have simpler

drive-mechanism components, with the force limited only by the air-pressure capabilities of the system. In contrast, mechanically driven mechanisms have smaller and more complex components, providing better spatial control but often with reduced maximum force capabilities. The cell viability rate after extrusion bioprinting typically ranges from 40% to 80%. However, maintaining high cell viability can be achieved by using low pressure and larger nozzles, though this may compromise resolution and printing speed. A CAD file is imported in STL file format and printed according to the required structure in fabrication. Technological advancements now allow multiple printheads to deposit multiple bioinks simultaneously, offering benefits such as control over porosity, shape, and cell distribution in fabricated parts (Vanaei et al., 2021).

Inkjet bioprinting use either thermal or acoustic inkjet to eject small bioink drops, as shown in Figure 1.8B. In piezoelectric inkjet bioprinters, a piezoelectric actuator generates acoustic waves through the bioink chamber, guiding and propelling the bioink through the printer nozzle. In contrast, thermal inkjet printers use an electrically heated print head to create air pressure pulses that expel the bioink. Studies indicate that the temperature of heating can be range from 200 °C to 300 °C and the overall temperature rises from 4 °C to 10 °C in a short duration (~ 2 µs). However, this heating does not adversely affect the stability of biological molecules, such as deoxyribonucleic acid (DNA) or the viability and function of mammalian cells post-printing (Goldmann and Gonzalez, 2000; Okamoto et al., 2000). Inkjet bioprinting offers advantages such as rapid printing speed, affordability, and widespread accessibility. However, it also has considerable limitations including potential exposure of cells and materials to thermal and mechanical stress, challenges with droplet directionality and uniform size, frequent nozzle clogging, and unreliable cell encapsulation.

A laser-assisted bioprinter consists of a pulsed laser beam, a focusing system, and a 'ribbon' that serves as a donor transport support typically made of glass, coated with a laser-energy-absorbing layer (e.g., gold or titanium). This ribbon also holds a layer of biological material (e.g., cells and/or hydrogel) prepared in a liquid solution. A receiving substrate is positioned opposite the ribbon to receive the printed material. Figure 1.8C illustrates this setup. Laser-assisted bioprinting functions by focusing laser pulses onto the absorbing layer of the ribbon, generating a high-pressure bubble that propels cell-containing materials toward a collector substrate (Murphy and Atala, 2014).

STL, or stereolithography, involves bioprinting by solidifying a bioink layer by layer through photopolymerisation, guided by a movable stage along the z-axis (Figure 1.8D). This method projects a 2D pattern onto the bioink reservoir, eliminating the need for an x-y printhead and enabling the fabrication of complex 3D structures. This feature contributes to a faster bioprinting rate compared to nozzle-based bioprinters. These systems maintain relatively high cell viability (>90%) by selectively crosslinking bioink with light, minimising shear stress on cells (Mandrycky et al., 2016). However, a significant limitation is the requirement for transparent liquid with minimal scattering to ensure even crosslinking; otherwise, irregular crosslinking may occur due to uneven light penetration. Nevertheless, STL has garnered significant interest across various fields for its ability to rapidly bioprint shapes with high resolution (around 1 µm) while preserving cell integrity (Kyle et al., 2017; Raman et al., 2016).

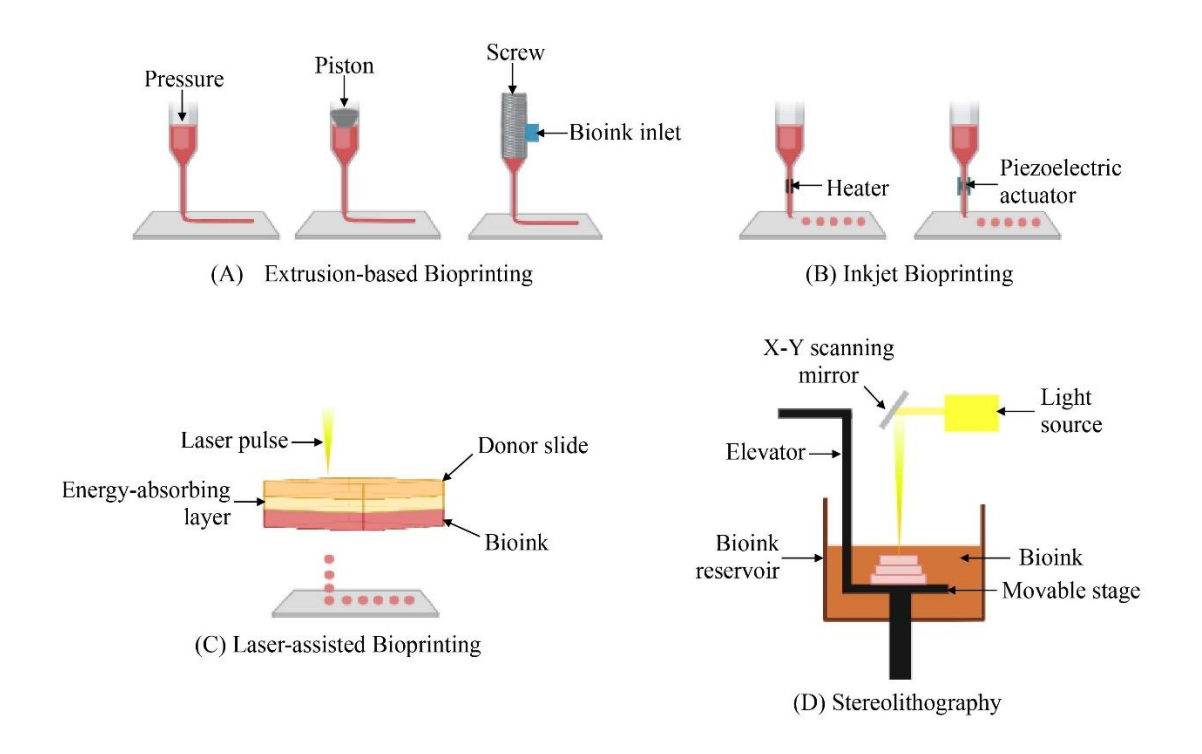


Figure 1.8 Schematic diagram of bioprinting techniques. (A) Extrusion-based Bioprinting (B) Inkjet Bioprinting (C) Laser-assisted Bioprinting and (D) Stereolithography.

1.5.6 Application of 3D bioprinting in glioblastoma

Currently, alginate is widely used as a bioink in the construction of 3D bioprinted glioblastoma model, with or without other components. According to Wang et al., (2021), combining alginate with gelatine provides good shear-thinning qualities, sufficient mechanical strength after crosslinking, and good physicochemical properties. Alginate has also been incorporated into hydrogels with fibrin and genipin, where fibrin enhances the development of stem cells and tumorigenic cells (C. Lee et al., 2019; Smits et al., 2020).

Wang et al., (2019) employed gelatine, alginate, fibrinogen and transglutaminase to construct a 3D bioprinted glioblastoma model and evaluated the sensitivity of 3D cells to chemotherapeutic drug temozolomide, as well as their in vivo tumourigenicity properties. They found that the 3D cultured glioblastoma cells with enhanced stemness properties exhibited increased drug resistance in vitro and

tumourigenicity in vivo. Han et al., (2020) constructed glioblastoma microenvironment by bioprinting a blood vessel layer comprising fibroblasts and endothelial cells in gelatine, alginate, and fibrinogen, followed by seeding multicellular glioblastoma tumour spheroids onto the blood vessel layer. They reported the generation of blood vessel sprouts and an increase in spheroid size.

The studies on 3D bioprinted glioblastoma models have advanced our understanding of bioink fabrication techniques and the characteristics and efficacy of bioinks. However, the application of 3D bioprinting technology for glioblastoma research is hindered by the consistent use of a limited range of bioink materials, predominantly alginate alone (Chaicharoenaudomrung et al., 2019; Utama et al., 2020; X. Wang et al., 2018b) or in combination with gelatine and fibrin (Dai et al., 2016; Han et al., 2020; X. Wang et al., 2018a, 2019). Furthermore, most studies on 3D glioblastoma models are typically conducted over relatively short periods (not exceeding 15 days), with Chaicharoenaudomrung et al., (2019) being an exception (21 days). Ongoing innovation in bioink development is crucial for advancing the field of 3D bioprinting. Novel bioinks capable of supporting long-term cultures are essential to expand the scope of research and clinical applications.

CHAPTER 2

METHODOLOGY

2.1 Experimental design

Figure 2.1 shows the flow chart of the study investigating the effectiveness of our own formulated bioink hydrogels in developing glioblastoma tumour microenvironment using 3D bioprinting.

In this study, the independent variables were the compositions of the bioink hydrogels, while the dependent variable was the efficacy of the bioink hydrogels in fabricating 3D bioprinted glioblastoma models. Different hydrogel compositions were formulated, for examples, alginate alone (ALG), a combination of alginate and chitosan (ALG-CHI), and a combination of alginate, chitosan and hyaluronic acid (ALG-CHI-HA). To study the effectiveness of the bioink hydrogels, the physical properties and the cell-matrix interaction of bioink groups (ALG, ALG-CHI and ALG-CHI-HA) were tested.

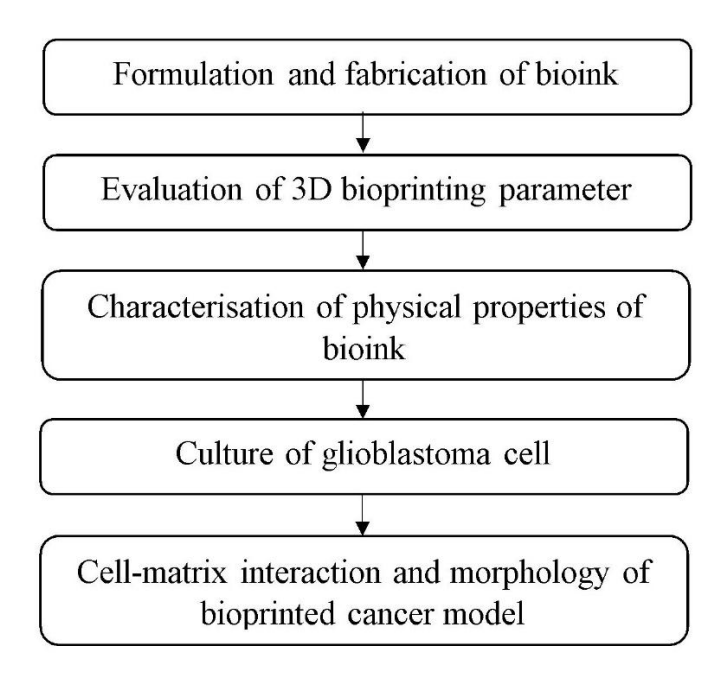


Figure 2.1 Flow chart of the study.